High Strain-Rate Compressive Properties of Carbon/Epoxy Laminated Composites – Effects of loading direction and temperature

Kenji Nakai[1,*], *Tsubasa* Fukushima[1], *Takashi* Yokoyama[1], and *Kazuo* Arakawa[2]

[1] Department of Mechanical Engineering, Okayama University of Science, Japan
[2] Research Institute for Applied Mechanics, Kyushu University, Fukuoka, Japan

Abstract. The high strain-rate compressive characteristics of a cross-ply carbon/epoxy laminated composite in the three principal material directions or fibre (1-), in-plane transverse (2-) and through-thickness (3-) directions are investigated on the conventional split Hopkinson pressure bar (SHPB) over a range of temperatures between 20 and 80 °C. A nearly 10 mm thick cross-ply carbon/epoxy composite laminate fabricated using vacuum assisted resin transfer molding (VaRTM) was tested. Cylindrical specimens with a slenderness ratio (= length/diameter) of 0.5 are used in high strain-rate tests, and those with the slenderness ratios of 1.0 and 1.5 are used in low and intermediate strain-rate tests. The uniaxial compressive stress-strain curves up to failure at quasi-static and intermediate strain rates are measured on an Instron testing machine at elevated temperatures. A pair of steel rings is attached to both ends of the cylindrical specimens to prevent premature end crushing in the 1- and 2- direction tests on the Instron testing machine. It is shown that the ultimate compressive strength (or failure stress) exhibits positive strain-rate effects and negative temperature ones over a strain-rate range of 10^{-3} to 10^{3}/s and a temperature range of 20 to 80 °C in the three principal material directions.

1 Introduction

In recent years, composite materials are increasingly replacing conventional metallic materials in aerospace, civil, marine and automotive industries, because of their higher specific strength and stiffness, higher fatigue properties and corrosion resistance. Composite structures in service conditions are often subjected to dynamic loading and temperature changes. It is, therefore, required to characterize the dynamic mechanical behaviour at elevated temperatures of composite materials. Excellent reviews on high strain-rate testing of composite materials can be found in the review articles [1–4]. The impact compressive [5–9], tensile [10–12] and shear [13, 14] stress–strain properties of composite materials were accurately determined using the classic [15] or modified split Hopkinson pressure bar (SHPB). However, except for Ref. [7], the effects of loading direction and temperature on their impact stress–strain behaviour have not been well investigated.

The primary objective of the present work is to determine the high strain-rate compressive properties of a cross-ply carbon/epoxy laminated composite in the three principal material directions or fibre (1-), in-plane transverse (2-) and through-thickness (3-) directions at elevated temperatures using the SHPB. Cylindrical specimens machined from a cross-ply composite laminate were used in both static and impact tests. The temperature dependence of the compressive stress–strain curves at low and intermediate strain rates were measured with an Instron 5500R testing machine. The respective influences of strain rate, loading direction and temperature on the ultimate compressive strength and strain, and absorbed energy up to failure were examined.

2 Experimental procedure

2.1 Test composite and specimen preparation

The nearly 10 mm thick cross-ply carbon/epoxy composite laminate ($[0/90]_{8S}$) fabricated using vacuum assisted resin transfer molding (VaRTM) was tested at room and high temperatures. The types of reinforcing fibre, matrix resin and fibre volume ratio are given in Table 1. Specimens were core-drilled out of the composite laminate along the three principal material directions and machined into small solid cylinders with a diameter (d) of 8 mm. After machining, the end surfaces of the specimen were carefully polished to a surface roughness of approximately 0.4 ~ 0.6 μm Ra with emery papers. The slenderness ratios of the static specimens were taken as l/d = 1.0 and 1.5. The slenderness ratio of 1.5 or 2.0 is recommended in the ASTM Designation E9-89a [16], while that of the impact specimen was taken as l/d = 0.5. This is because the slenderness ratios of 0.5 or less can be effective in the SHPB testing of

* Corresponding author: nakai@mech.ous.ac.jp

low-impedance materials to minimize wave attenuation in the specimen [17].

Table 1. Types of reinforcing fibre and matrix resin used in cross-ply carbon/epoxy laminated composite.

	Cross-ply carbon/epoxy laminated composite
Fibre	HTS40 F13 12K (Toho Tenax)
Matrix	Epoxy XNR/H 6815
Fibre volume ratio V_f	0.56

2.2 Low and intermediate strain-rate testing

Low and intermediate strain-rate compression tests (see, Fig. 1) were performed using the cylindrical specimens with l/d = 1.0 and 1.5 on the Instron 5500R testing machine at two different crosshead speeds V_c of 1 and 50 mm/min over the temperature range 20 to 80 °C. Both ends of the static specimen were lubricated with molybdenum disulfide (MoS_2) to minimize frictional effects between the specimen and the loading anvils. We used an environmental chamber to heat the specimen. In order to measure the specimen temperature, the thermocouple was attached to the specimen surface. In the 1- and 2- direction tests, steel rings [18] (see, Figs. 1 and 2), consisting of a 3 mm thick circular steel plate with a diameter of 30 mm and a 8.0 mm circular cutout in the centre, were attached at both ends of the cylindrical specimen to prevent premature kink band formation or longitudinal splitting near the specimen ends. Compressive stress in the specimen was determined using a 100-kN capacity load cell (Instron: Model 2525-801). Compressive strain in the specimen was determined using an extensometer (Instron: Model 2620-601).

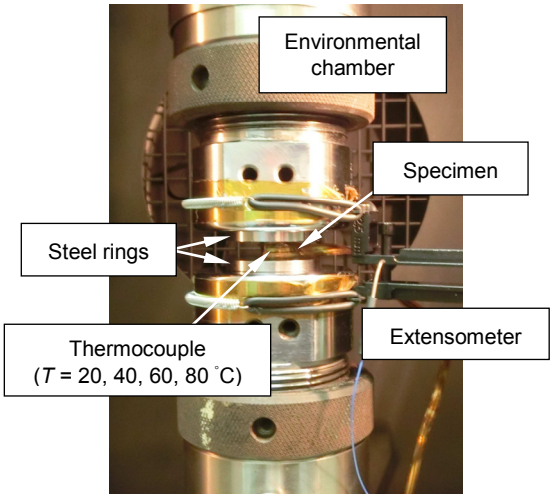

Fig. 1. Static compression tests on cross-ply CFRP specimen in fibre (1-) and in-plane transverse (2-) directions at elevated temperatures.

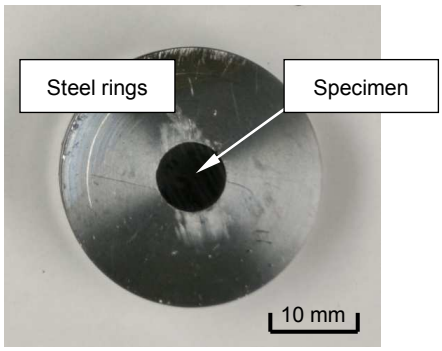

Fig. 2. Steel rings attached to both ends of cylindrical specimen.

2.3 Split Hopkinson pressure bar testing

Figure 3 shows a schematic of the standard SHPB system. The SHPB system consists principally of high-carbon bearing steel input and output bars, a high-carbon bearing steel striker bar, a gun barrel and an associated recording system (not shown here). The specimen was sandwiched between the input and output bars. In order to heat the specimen, we used an electric furnace with a temperature controller. As in the low and intermediate strain-rate tests, the thermocouple was attached to the specimen surface. Lubricant (or MoS_2) was applied to the two bar/specimen interfaces to reduce the frictional effects. A pulse shaping technique [19] was used to generate well-defined compressive strain pulses without higher frequency components in the input bar. Namely, a 0.4 mm-thick steel disk of nearly 16 mm in diameter was attached onto the impact (left) end of the input bar using a thin layer of petroleum jelly. Details of the test procedure can be found elsewhere [9].

From one-dimensional elastic wave propagation theory, we can determine the nominal strain $\varepsilon(t)$, strain rate $\dot{\varepsilon}(t)$ and stress $\sigma(t)$ in the specimen from the SHPB test records as [20]

$$\varepsilon(t) = \frac{u_1(t) - u_2(t)}{l} = \frac{2c_o}{l}\int_0^t \{\varepsilon_i(t') - \varepsilon_t(t')\}\mathrm{d}t' \quad (1)$$

$$\dot{\varepsilon}(t) = \frac{\dot{u}_1(t) - \dot{u}_2(t)}{l} = \frac{2c_o}{l}\{\varepsilon_i(t) - \varepsilon_t(t)\} \quad (2)$$

$$\sigma(t) = \frac{P_2(t)}{A_S} = \frac{AE}{A_S}\varepsilon_t(t) \quad (3)$$

Here u and P are the displacement and the axial force on both ends of the specimen (where subscripts 1 and 2 denote the left and right interfaces, respectively); an overdot denotes the time derivative; A, E and c_o are the cross-sectional area, Young's modulus (= 209 GPa) and the longitudinal elastic wave velocity of the Hopkinson bars; A_S is the cross-sectional area of the specimen. Equations (1) to (3) are derived on the assumption of dynamic force equilibrium across the specimen, i.e.,

$$P_1(t) = P_2(t) \quad \text{or} \quad \varepsilon_i(t) + \varepsilon_r(t) = \varepsilon_t(t) \quad (4)$$

where

$$P_1(t) = AE[\varepsilon_i(t) + \varepsilon_r(t)], \quad P_2(t) = AE\varepsilon_t(t)$$

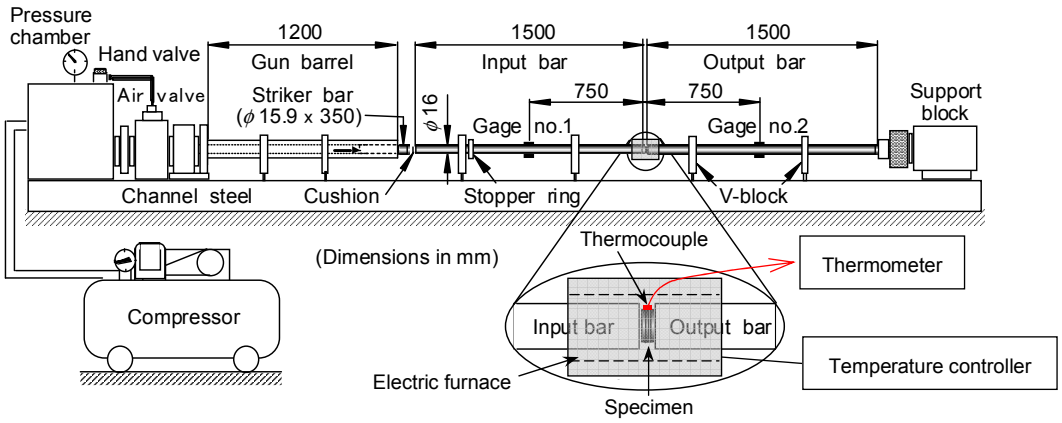

Fig. 3. Schematic diagram of standard SHPB apparatus (recording system not shown).

In the above derivations, the incident and reflected strain pulses are time-shifted to the specimen-input bar interface, and the transmitted strain pulse is time-shifted to the specimen-output bar interface. Eliminating time t through Equations (1) to (3) yields the nominal (or engineering) compressive stress–strain and strain rate–strain relations. The compression is taken as positive in this study.

3 Results and discussion

3.1 Effect of strain rate

A number of the SHPB tests were conducted at room and high temperatures. Figure 4 indicates typical oscilloscope records of strain gage outputs from the 3-direction SHPB test at room temperature. The top trace gives the incident and reflected strain pulses (ε_i and ε_r), and the bottom trace gives the strain pulse (ε_t) transmitted through the specimen. The output signals from the strain gages were recorded at a sampling rate of 1 MHz. The recorded signal data are neither smoothed nor averaged electronically. Figure 5 gives the resulting axial stress histories at the front and back ends of the specimen, indicating that dynamic stress equilibrium is achieved in the specimen over the entire loading duration. The failure initiation in the specimen took place at the peak stress (corresponding to the ultimate compressive strength σ_C) at 118μs. Figure 6 depicts the resulting impact compressive stress–strain and strain rate–strain relations. Note that the strain rate does not remain constant during the test, and, hence, the strain rate $\dot{\varepsilon}$ = 790/s given indicates the average one up to failure. There is an abrupt increase in the strain rate at point X on the stress–strain curve, corresponding to the failure initiation. Figure 7 presents typical compressive stress–strain curves in the 1-, 2- and 3- directions at two different strain rates at room temperature. The ultimate compressive strength σ_C increases slightly, while the ultimate compressive strain ε_C decreases greatly with increasing strain rate. The absorbed energy U_C is obtained by numerical integration of the compressive stress–strain curve up to ε_C measured in the static and impact tests. In order to discuss the effects of strain rate and loading direction along the three principal material axes on the compressive properties, σ_C, ε_C and U_C at room temperature are plotted in Figs. 8 to 10 against a newly defined strain rate at failure $\dot{\varepsilon}_f = \varepsilon_C / t_f$ (t_f: failure initiation time).

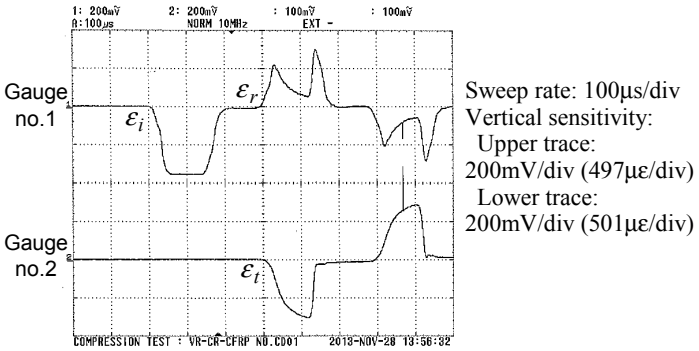

Fig. 4. Oscilloscope traces from 3-direction SHPB test on cross-ply carbon/epoxy laminated composite at room temperature (V_S = 8.1 m/s).

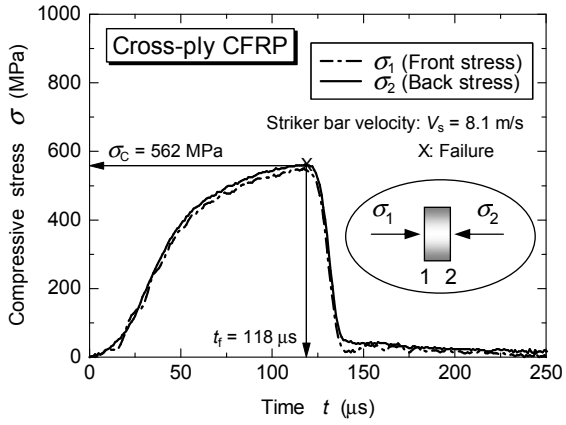

Fig. 5. Axial compressive stress histories at front and back ends of specimen in 3-direction at room temperature.

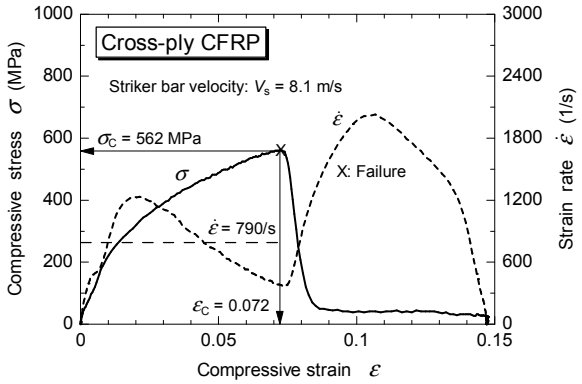

Fig. 6. Impact compressive stress–strain and strain rate–strain relations for cross-ply carbon/epoxy laminated composite in 3-direction at room temperature.

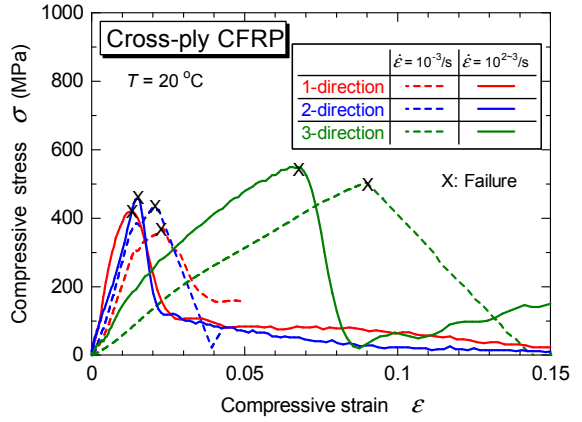

Fig. 7. Compressive stress–strain curves for cross-ply carbon/epoxy laminated composite at two different strain rates in three principal material directions at room temperature.

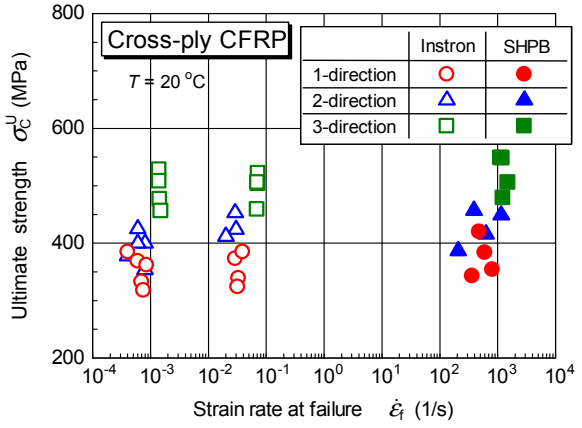

Fig. 8. Ultimate compressive strength (failure stress) versus strain rate at failure in three principal material directions at room temperature.

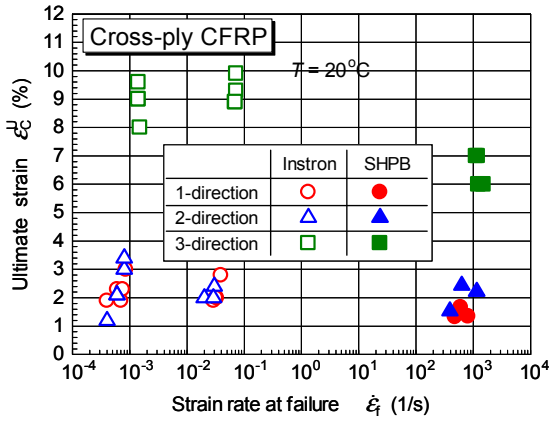

Fig. 9. Ultimate compressive strain (failure strain) versus strain rate at failure in three principal material directions at room temperature.

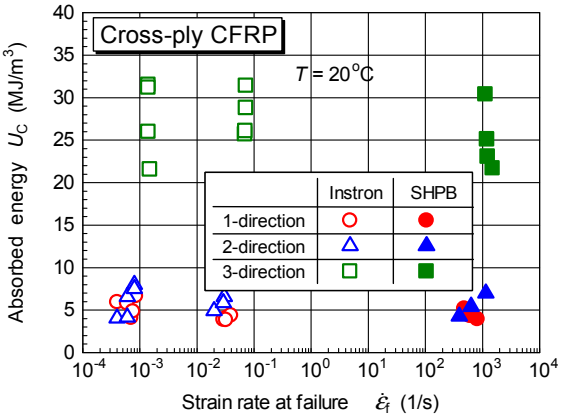

Fig. 10. Absorbed energy up to failure versus strain rate at failure in three principal material directions at room temperature.

The ultimate compressive strength σ_C exhibits a positive strain-rate dependence. This may be due to the viscoelastic nature of the epoxy resin matrix itself [6]. In contrast, the ultimate compressive strain ε_C and absorbed energy U_C up to failure exhibit a negative strain-rate dependence. The compressive properties in the 3-direction are much higher than those in the 1- and 2-directions at any strain rate.

3.2 Effect of temperature

Figure 11 shows the static and impact compressive stress–strain curves at two different temperatures in the 2- and 3- directions. The initial modulus and ultimate strength decrease greatly, while the ultimate strain increases slightly with increasing temperature. In order to discuss the effects of temperature and loading direction on the compressive properties, σ_C, ε_C and U_C are plotted in Figs. 12 to 14 against temperature. At low strain rates ($\dot{\varepsilon}$ = 10^{-3}/s), the ultimate strength decreases rapidly at temperatures above 60 °C in the 1- and 2-directions. This is because it is close to the glass

transition temperature T_g (= 90 °C) of the epoxy resin used as the matrix. However, in the 3-direction, we cannot see the rapid decrease in the ultimate strength at high temperatures. This may be because the through-thickness compressive strength is significantly affected by the fibre properties.

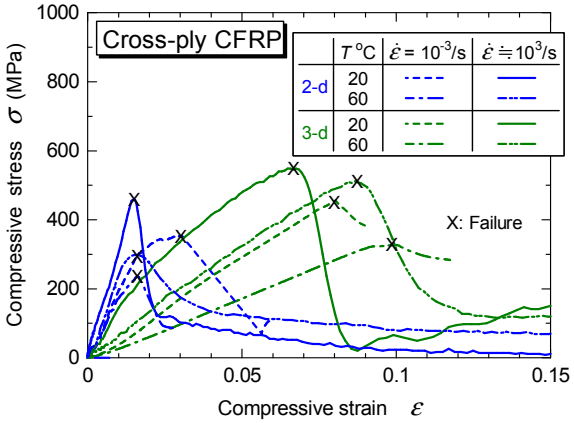

Fig. 11. Static and impact compressive stress–strain relations for cross-ply carbon/epoxy laminated composite at two different temperatures in 2- and 3- directions.

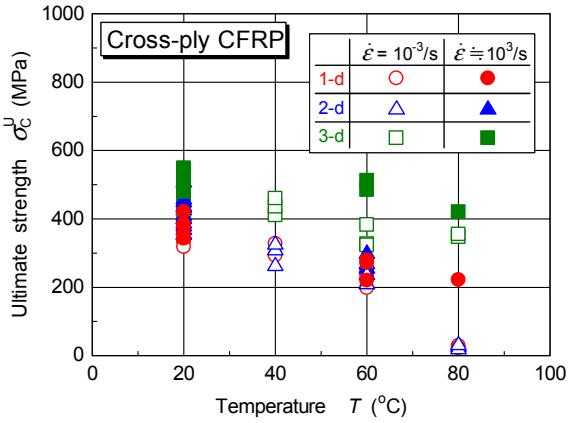

Fig. 12. Ultimate compressive strength (failure stress) versus temperature in three principal material directions at low and high strain rates.

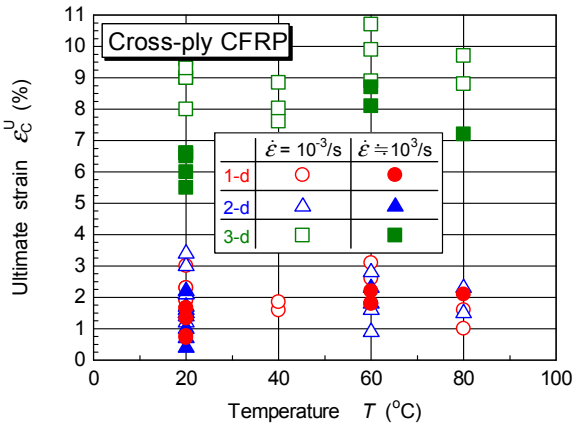

Fig. 13. Ultimate compressive strain (failure strain) versus temperature in three principal material directions at low and high strain rates.

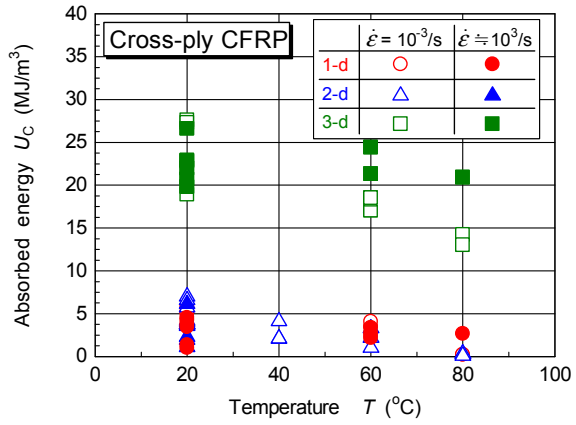

Fig. 14. Absorbed energy up to failure versus temperature in three principal material directions at low and high strain rates.

In an attempt to discuss the temperature dependence of the ultimate strength, we observed the failure modes of the static specimens at room and high temperatures. Figures 15 and 16 indicate the pictures of the specimens after static testing at four different temperatures in the 2- and 3- directions. In the 2- direction, the specimens fail by the creation of only one shear failure surface at T = 20~60 °C. Meanwhile, at high temperatures (T = 80 °C), we can observe the fibre buckling caused by the softening of the matrix. In the 3- direction, the specimens fail by shear failure at T = 20 °C. In contrast, at high temperatures (T = 40~80 °C), the specimens fail by crushing and multiple shearing.

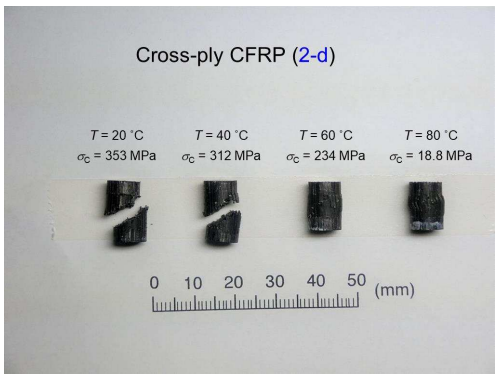

Fig. 15. Pictures of specimens after static testing at four different temperatures in 2- direction.

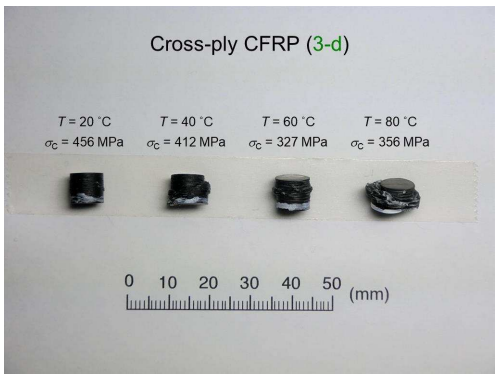

Fig. 16. Pictures of specimens after static testing at four different temperatures in 3- direction.

4 Conclusions

The effects of strain rate, loading direction and temperature on the compressive stress–strain characteristics of the cross-ply carbon/epoxy laminated composite fabricated by VaRTM have been examined in detail. From the present experimental investigation, we can draw the following conclusions:

(1) The ultimate compressive strength (or failure stress) increases marginally, while the ultimate compressive strain and absorbed energy decrease significantly with strain rate in the range of 10^{-3} to 10^{3}/s in the three principal material directions.

(2) The compressive properties in the 3- direction are even higher than those in the 1- and 2- directions at low and high rates of strain.

(3) The ultimate compressive strength decreases greatly with increasing temperature. In particular, in the 1- and 2- directions, the ultimate strength decreases rapidly at low strain rates and high temperatures.

(4) The failure surfaces are strongly affected by the temperature as well as loading directions.

This work was supported in part by the Collaborative Research Program of Research Institute for Applied Mechanics, Kyushu University.

References

1. R.L. Sierakowski, Appl. Mech. Rev., **50**, 741 (1997)
2. A.M.S Hamouda, M.S.J. Hashmi, J. Mater. Process. Technol., **77**, 327 (1998)
3. T. Yokoyama, J. JSEM (in Japanese), **6**, 105 (2006)
4. J.V. Blitterswyk, L. Fletcher, F. Pierron, Adv. Exp. Mech., **2**, 3 (2017)
5. J. Harding, Composites, **24**, 323 (1993)
6. T.E. Tay, H.G. Ang, V.P.W. Shim, Compos. Struct., **33**, 201 (1995)
7. N. Takeda, L. Wan, M. Hiramatsu, J. Yuan, Trans. Jpn. Soc. Mech. Eng. A (in Japanese), **63**, 2598 (1997)
8. M.V. Hosur, J. Alexander, U.K. Vaidya, S. Jeelani, Compos. Struct., **52**, 405 (2001)
9. T. Yokoyama, Appl. Mech. Mater., **1/2**, 11 (2004)
10. J. Harding, L.M. Welsh, J. Mater. Sci., **18**, 1810 (1983)
11. G.H. Staab, A. Gilat, J. Compos. Mater., **29**, 1308 (1995)
12. R. Gerlach, C.R. Siviour, J. Wiegand, N. Petrinic, Mech. Adv. Mater. Struct., **20**, 505 (2013)
13. S.M. Werner, C.K.H. Dharan, J. Compos. Mater., **20**, 365 (1986)
14. J. Harding, Y.L. Li, Compos. Sci. Technol., **45**, 161 (1992)
15. H. Kolsky, Proc. Phys. Soc., **B62**, 676 (1949)
16. ASTM E9-89a, *Annual book of ASTM standards*, Vol.03.01 (American Society for Testing and Materials, Philadelphia, 1995)
17. G.T. Gray III, *ASM Handbook, Vol.8, Mechanical Testing and Evaluation* (ASM International, Materials Park, OH, 2000)
18. J. Lankford, Adv. Compos. Mater., **19**, 553 (1991)
19. B. Song, W. Chen, Exp. Mech., **44**, 622 (2004)
20. U.S. Lindholm, J. Mech. Phys. Solids, **12**, 317 (1964)